



Cite this: *Polym. Chem.*, 2024, **15**, 422

## **π-Face strapped monomers enable self-stabilized hyperbranched π-conjugated polymer particles†**

Manikandan Mohanan,<sup>a,b</sup> Xinran Zhang<sup>b,c</sup> and Nagarjuna Gavvalapalli  <sup>a,b</sup>

π-Conjugated polymers that extend the π-conjugation in more than one dimension are highly sought after for various organic electronic and energy applications. However, the synthesis of solution processable higher dimensional π-conjugated materials is still at its infancy because of strong interchain π–π interactions. The conventional strategy of using linear alkyl pendant chains does not help overcome the strong interchain π–π interactions in higher dimensional π-conjugated materials as they do not directly mask the π-face of the repeat units. While the miniemulsion technique has been employed to generate hyperbranched π-conjugated polymer particles stabilized by surfactants, this approach does not address the molecular level challenges. We have proposed that π-face masking straps mask the π-face of the polymer backbone and therefore help to control π–π interchain interactions in higher dimensional π-conjugated materials at the molecular level. Herein, we have shown that when a strapped aryl dialdehyde monomer ( $A_2$ ) is reacted with a trifunctional 1,3,5-benzenetriamine ( $B_3$ ) using dynamic imine chemistry, a solution dispersible and processable hyperbranched polymer with a degree of branching of 0.46 is generated. Also, by varying the reaction conditions (catalyst, monomer concentration, and solvent), solution dispersible polymer particles of varying diameters ranging from 60 to 300 nm are generated. It is worth noting that despite having the suitable monomer architectures for the formation of ordered frameworks, a hyperbranched polymer is generated because the straps effectively hinder interlayer π–π stacking interactions, thereby preventing the formation of crystalline aggregates that are required for the growth of the former. Since straps stabilize the chains against π–π interactions at the molecular level, they will not only provide synthetic control over the architecture but also remove typical synthetic limitations associated with the miniemulsion technique including functional group intolerance and monomer miscibility.

Received 18th October 2023,  
Accepted 20th December 2023

DOI: 10.1039/d3py01158e

[rsc.li/polymers](http://rsc.li/polymers)

## Introduction

Delocalization of π-electrons along the polymer backbone makes π-conjugated polymers useful for several applications including organic electronics, energy and sensors.<sup>1–5</sup> Extending this delocalization into multiple dimensions unlocks intriguing electronic and optoelectronic characteristics in higher dimensional π-conjugated materials.<sup>6–15</sup> However, controlling polymer growth beyond one dimension and synthesizing solution-processable higher dimensional π-conjugated polymers have been persistent challenges in materials science due to strong interchain van der Waals and π–π interactions in these

materials.<sup>11,15,16</sup> The conventional use of linear alkyl pendant chains, which effectively renders 1D-π-conjugated polymers soluble, does not directly shield the π-faces of repeat units and hence fails to address the strong interchain π–π interactions encountered in higher dimensional π-conjugated materials.<sup>17,18</sup> As a result, a prevalent approach to generate solution-processable networks and hyperbranched polymers (HBPs) involves the utilization of the miniemulsion technique.<sup>19–25</sup> In this method, surfactants are used to stabilize the polymer particles against aggregation. However, surfactants do not confer solubility at the molecular level, posing challenges in controlling polymer growth and branching. Furthermore, the presence of surfactants on the nanoparticles can adversely affect the optical and electronic properties of the polymer. Alternative synthetic strategies, such as using non-stoichiometric monomer feed ratios and using synthetically demanding  $AB_2$  type monomers in conjunction with pendant alkyl chains, have shown success in producing soluble low molecular weight π-conjugated HBPs.<sup>15,26–28</sup> Although some progress has been made in synthesizing solution-processable conjugated HBPs by mitigating interchain interactions through interarylene torsion angles and pendant

<sup>a</sup>Department of Chemistry, Georgetown University, Washington, DC, USA.  
E-mail: [ng554@georgetown.edu](mailto:ng554@georgetown.edu)

<sup>b</sup>Institute for Soft Matter Synthesis and Metrology, Georgetown University, Washington, DC, USA

<sup>c</sup>Department of Physics, Georgetown University, Washington, DC, USA

† Electronic supplementary information (ESI) available. CCDC 2266289. For ESI and crystallographic data in CIF or other electronic format see DOI: <https://doi.org/10.1039/d3py01158e>

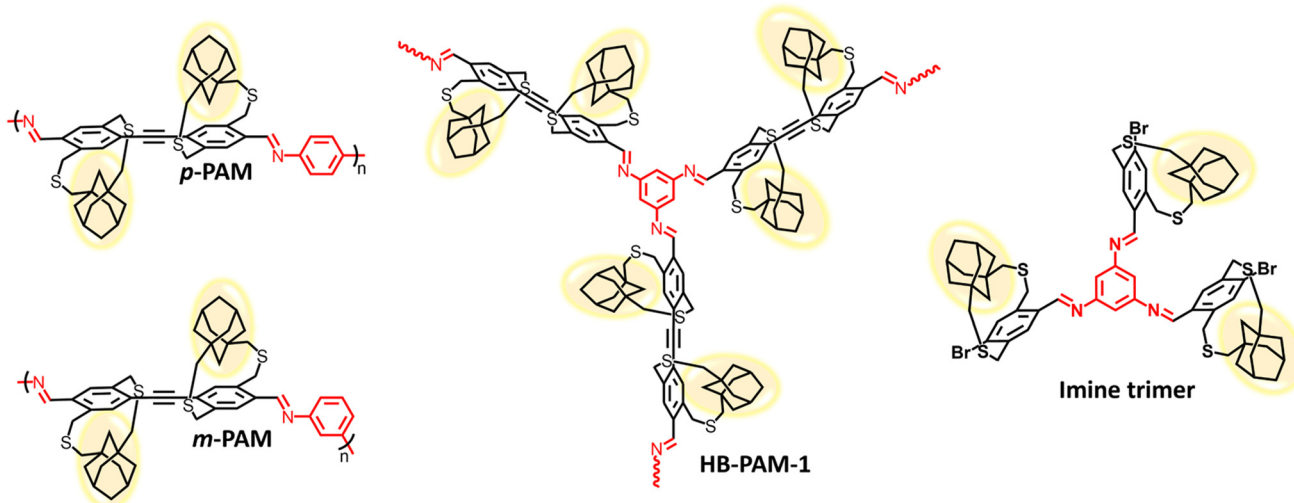


**Fig. 1** Chemical structures of the linear polyazomethines (*p*-PAM and *m*-PAM), the hyperbranched polyazomethine (HB-PAM-1) and the model imine trimer synthesized and studied in this work.

solubilizing chains,<sup>19,29–31</sup> there remains a critical need for strategies that directly target the interchain  $\pi$ – $\pi$  stacking interactions at the molecular level, enabling control over the growth and processability of  $\pi$ -conjugated HBPs.

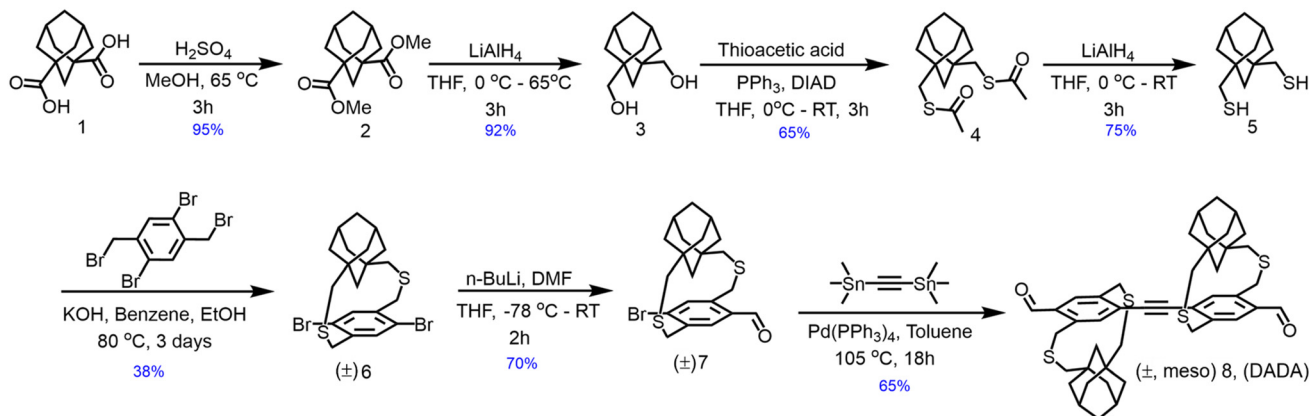
Several groups have used  $\pi$ -face masking straps to enhance  $\pi$ -conjugated polymer's chemical stability, photostability, fluorescence quantum yield, electroluminescence, and intrachain charge transport.<sup>32–36</sup> Our research group has been focused on designing and developing  $\pi$ -face masking straps that overcome interchain interactions, allow the solution phase synthesis of higher dimensional  $\pi$ -conjugated materials and generate soluble higher dimensional materials. Unlike traditional linear pendant alkyl chains, these novel  $\pi$ -face masking straps directly shield the  $\pi$ -face of the repeat unit and effectively overcome interchain  $\pi$ – $\pi$  interactions. Our research group has been at the forefront of this field and demonstrated the efficacy of cycloalkyl straps by the design and synthesis of  $\pi$ -face masking straps that enable the production of soluble, high molecular weight linear polymers (*ca.* 24 kDa) and two-dimensional  $\pi$ -conjugated oligomers, without the need for pendant solubilizing chains.<sup>37–40</sup> Furthermore, we successfully synthesized conjugated porous polymer networks using adamantly strapped building blocks and irreversible P–C bond forming reactions.<sup>41</sup> The incorporation of adamantly straps not only reduced interchain  $\pi$ – $\pi$  interactions but also enhanced the residence time of the network in the reaction mixture, resulting in a swollen network that allowed monomers to diffuse and react, enabling control over the network size and crosslinking density.<sup>41</sup>

In this work, we report the synthesis of linear and hyperbranched strapped-polyazomethines by harnessing the power of strapped building blocks and dynamic imine chemistry.<sup>42</sup> By employing imine condensation polymerization, we successfully polymerized a strapped aryl dialdehyde monomer ( $A_2$ ) with difunctional aryl amines ( $B_2$ ), resulting in the production

of high molecular weight linear polyazomethines (*p*-PAM and *m*-PAM) (Fig. 1). The synthesis of linear polymers played a pivotal role in the subsequent synthesis and structural characterization of strapped-hyperbranched polymers. Utilizing the knowledge gained from linear polymer synthesis, the strapped aryl dialdehyde monomer ( $A_2$ ) was copolymerized with a trifunctional aryl amine unit ( $B_3$ ) to generate solution-dispersible and -processable hyperbranched polyazomethines (HB-PAMs) without the necessity of incorporating pendant solubilizing chains or surfactants (Fig. 1). By carefully controlling key polymerization conditions, such as the selection of the catalyst, monomer concentration, and solvent, we were able to control the growth and morphology of the resulting HB-PAM particles.

## Results and discussion

In this work, an adamantly-strapped monomer was selected as the aryl-strapped building block due to its demonstrated efficiency in hindering interchain interactions compared to the cyclohexyl-strapped monomer.<sup>37</sup> Additionally, dynamic imine chemistry<sup>42</sup> was used here to generate linear and hyperbranched polymers. The dynamic covalent chemistry enables reversible covalent bond formation reactions and has been utilized in various research areas to create elusive yet significant materials, such as macrocycles and covalent organic frameworks.<sup>43–50</sup> More importantly, the imine reaction facilitates the extension of  $\pi$ -conjugation between the building blocks.<sup>51–54</sup> Dibromoadamantanocyclophane (**6**) was synthesized from adamantan dicarboxylic acid (**1**) by following our previous synthetic protocols as shown in Scheme 1.<sup>37</sup> Compound **6** was converted into a bromoadamantanocyclophane carbaldehyde (**7**) and then subjected to Stille coupling with bis(trimethylstannyl)acetylene to produce diadamantan-



**Scheme 1** Synthesis of strapped aryl dialdehyde monomer ( $\pm$ , meso) 8 (DADA).

cyclophane dialdehyde, ( $\pm$ , meso) 8, (DADA) which serves as an  $\text{A}_2$  monomer for the linear polymer and HBP syntheses. DADA was synthesized and used as an  $\text{A}_2$  monomer rather than monoadamantyl dialdehyde to maintain a higher percentage of strapped monomers in the co-polymers and HBPs. Previously, we have shown that the strapped monomers generate soluble linear  $\pi$ -conjugated polymers of higher molecular weight without the need for pendant solubilizing chains and the incorporation of co-monomers that do not contain straps and solubilizing pendant chains will reduce polymer solubility.<sup>37,38</sup> Therefore, DADA, compared to the monoadamantyl dialdehyde, provides a higher percentage of the strapped repeat units in the linear co-polymers and HBPs, which will help to overcome interchain  $\pi$ - $\pi$  interactions and enable soluble polymers without pendant solubilizing chains. Also, DADA was obtained as a mixture of stereoisomers and used as is without chiral resolution. The presence of a mixture of stereoisomers of DADA in the polymerization mixture will generate an atactic polymer. Atactic polymers typically have higher solubility limits than iso- or syndio-tactic polymers obtained from chiral monomers. The crystal structure of DADA is shown in Fig. 2 and S1† (triclinic,  $P\bar{1}$ ).

There are no reports on the imine condensation polymerization of strapped monomers. Therefore, before pursuing the strapped HBP synthesis, we first aimed to optimize the imine condensation reaction conditions by synthesizing two linear polyazomethines, *para*-polyazomethine (*p*-PAM) and *meta*-polyazomethine (*m*-PAM). DADA was reacted with *p*-phenylene diamine to generate *p*-PAM using different catalysts and solvents as shown in Scheme 2 and Table 1. Polymerizations were typically run for 20 hours at  $50^\circ\text{C}$ , and the molecular weights of the resultant polymers were determined using GPC. The solvent for the polymerization was optimized by using zinc triflate as a catalyst at a constant monomer concentration of  $10 \text{ mg mL}^{-1}$ . It was observed that the mixture of acetonitrile (ACN) and  $\text{CHCl}_3$  in a 2:1 (v/v) ratio resulted in a high molecular weight (10.7 kDa) and mostly soluble polymer. Using this solvent combination, different Lewis acids and Brønsted-Lowry acids were screened as catalysts. Among the screened Lewis acids, boric

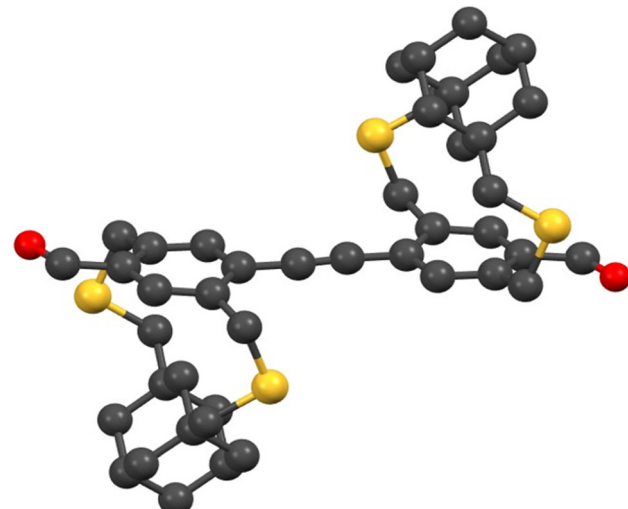
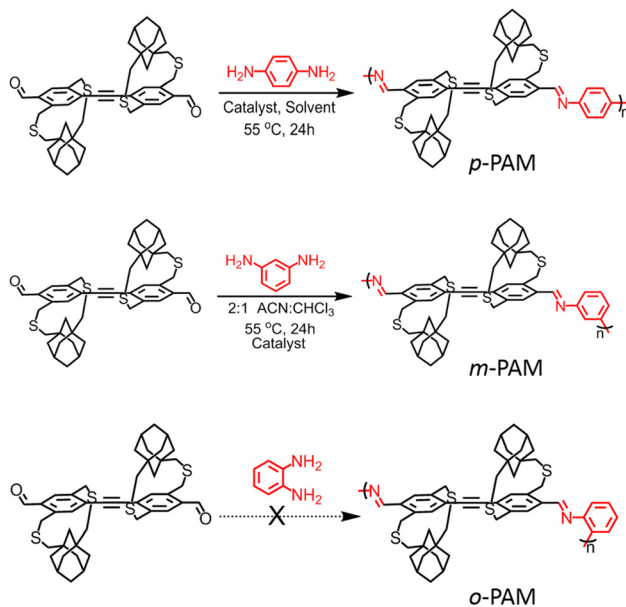


**Fig. 2** Crystal structure of DADA (black – C, yellow – S, and red – O; H atoms are omitted for clarity).

acid resulted in the highest molecular weight (*ca.* 19.2 kDa) polymer. And among the screened Brønsted-Lowry acids, acetic acid resulted in a high molecular weight (18.4 kDa) polymer. Stronger Brønsted-Lowry acids such as *p*-toluene sulfonic acid and trifluoroacetic acid resulted in the formation of an insoluble precipitate probably due to the formation of high molecular weight insoluble polymers.

The polymerization conditions optimized for synthesizing *p*-PAM were utilized for the synthesis of *m*-PAM. By reacting *m*-phenylenediamine and DADA in the presence of acetic acid and boric acid catalysts, *m*-PAM polymers with molecular weights of 17 and 31 kDa were successfully obtained. However, when boric acid was used as a catalyst, the yield of the soluble fraction was less than 20% for the 31 kDa *m*-PAM. On the other hand, maintaining the molecular weight below 20 kDa resulted in greater than 30% yield of the soluble polymer. It is worth noting that none of these conditions led to the formation of polymers greater than 1 kDa when DADA was



**Scheme 2** Synthesis of linear polyazomethines (PAMs).

reacted with *o*-phenylenediamine, likely due to steric hindrance. Therefore, the appropriate conditions for synthesizing strapped polyazomethines with a decent soluble fraction yield include running the imine condensation polymerization in a mixture of ACN and chloroform (2 : 1 v/v) with a DADA concentration of 10 mg mL<sup>-1</sup> in the presence of the acetic acid catalyst at 50 °C for 20 hours. Polymer structures were confirmed using ATR-IR (Fig. 3 and S2†) and <sup>1</sup>H NMR (Fig. S8 and S9†). In the ATR-IR spectra, a new peak at 1620 cm<sup>-1</sup> was observed (Fig. 3) for both *p*-PAM and *m*-PAM, which corresponds to the imine stretch and matches with the values reported in the literature.<sup>55–57</sup> Additionally, the presence of a peak at 8.9 ppm in the solution-state <sup>1</sup>H NMR spectra of the polyazomethines confirms the formation of imine bonds. The relatively low intensity peak at 10.35 ppm in the <sup>1</sup>H NMR spectra and the carbonyl stretch at around 1680 cm<sup>-1</sup> in the ATR-IR spectra are attributed to the terminal aldehyde groups on the polyazomethines. Thus, the strapped DADA monomer undergoes imine polymerization with *para*- and *meta*-phenylenediamines and generates relatively high molecular weight and soluble linear polyazomethines.

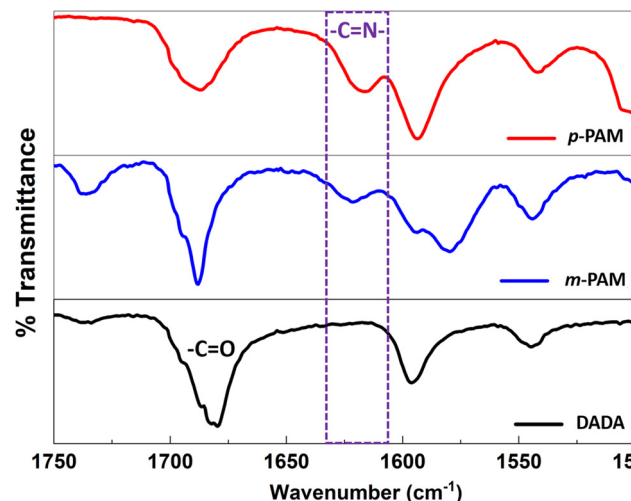


**Fig. 3** ATR-IR spectra of *p*-PAM, *m*-PAM and DADA.

The optimized conditions for imine condensation polymerization, which were established for the synthesis of linear polyazomethines, were utilized as the foundation for the synthesis of strapped conjugated HBPs using dynamic imine chemistry. DADA (A<sub>2</sub>) was reacted with 1,3,5-benzenetriamine (B<sub>3</sub>) under different conditions to generate conjugated hyperbranched polyazomethines (HB-PAMs) as shown in Table 2. The volume ratio of chloroform in the solvent mixture was increased for HBP synthesis since higher dimensional polymers typically have a lower solubility limit than the linear polymers. Two Lewis acids (zinc triflate and scandium triflate) and a Brønsted–Lowry acid were tested (Table 2) in a 1 : 1 (v/v) mixture of ACN and chloroform. Gelation of the reaction mixture occurred within 30 minutes when using both the Lewis acids. On the other hand, a solid precipitate was observed in the presence of acetic acid after 2 hours of polymerization. A relatively high concentration of the DADA monomer (12 mM) may have led to the formation of a cross-linked network in all three cases.

In order to control the polymer growth, avoid crosslinking and obtain a soluble material, the HBP was grown in a two-step process (Scheme 3; condition iv, Table 2). DADA (12 mM) was reacted with 1,3,5-benzenetriamine in an ACN : CHCl<sub>3</sub> (1 : 1 v/v) mixture for 90 minutes at 55 °C to form dispersible

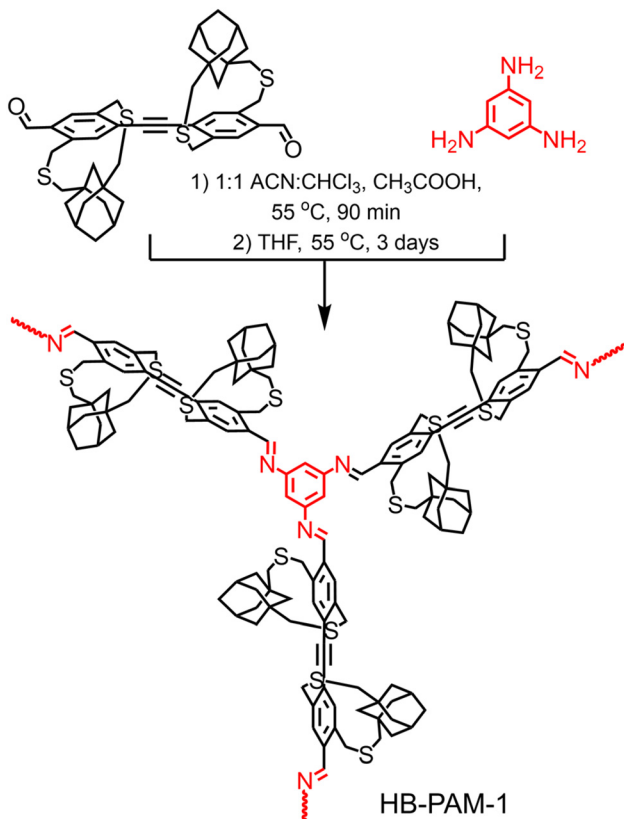
**Table 1** Solvent and catalyst optimization for the synthesis of *p*-PAMs

Solvent screening <sup>a</sup>	<i>M<sub>n</sub></i> <sup>b</sup> (kDa)	Catalyst screening <sup>c</sup>			
		Lewis acids	<i>M<sub>n</sub></i> <sup>b</sup> (kDa)	Brønsted–Lowry acids	<i>M<sub>n</sub></i> <sup>b</sup> (kDa)
4 : 1 Toluene : ACN	3.4	Copper(I) triflate	4.6	Acetic acid	18.4
Chloroform	5.1	Copper(II) triflate	3.9	Trifluoroacetic acid	Insoluble
1 : 2 ACN : CHCl <sub>3</sub>	3.0	Nickel(II) triflate	7.4	<i>p</i> -Toluene sulfonic acid	Insoluble
1 : 1 ACN : CHCl <sub>3</sub>	9.3	Zinc(II) triflate	10.7		
2 : 1 ACN : CHCl <sub>3</sub>	10.7	Scandium(III) triflate	16.1		
3 : 1 ACN : CHCl <sub>3</sub>	7.9	Boric acid	19.2		

<sup>a</sup> At a monomer concentration of 10 mg mL<sup>-1</sup> in presence of zinc triflate catalyst. <sup>b</sup> Tetrahydrofuran gel permeation chromatography with polystyrene standards. <sup>c</sup> At a monomer concentration of 10 mg mL<sup>-1</sup> in 2 : 1 ACN : CHCl<sub>3</sub>.

**Table 2** Screening of reaction conditions for the synthesis of HB-PAM at a constant monomer concentration of 12 mM

Solvent	Catalyst	Time	Observation
(i) 1 : 1 ACN : CHCl <sub>3</sub>	Zinc triflate	25 min	Gel
(ii) 1 : 1 ACN : CHCl <sub>3</sub>	Scandium triflate	20 min	Gel
(iii) 1 : 1 ACN : CHCl <sub>3</sub>	Acetic acid	24 h	Precipitate
(iv) 1 : 1 ACN : CHCl <sub>3</sub> /THF	Acetic acid	90 min/3 days	Dispersion (HB-PAM-1)



**Scheme 3** Synthesis of HB-PAM-1.

polymer particles. The solvent was removed under reduced pressure, and the residue was redispersed in THF and further reacted in the presence of the acetic acid catalyst at 55 °C for 3 days. The advantage of a two-step process is that, in the first step, dispersible nanosized HBP particles are generated. In the second step, the polymer can undergo restructuring due to the reversible nature of the imine reaction, while also continuing to grow further through polymerization. THF is selected as a solvent for the second step because it acts as a marginal solvent for strapped conjugated polymers. Consequently, when THF is used as a solvent, the HBP is expected to precipitate from the reaction mixture before it can grow into an insoluble high molecular weight network. At the end of the polymerization, THF was removed and the resultant precipitate was washed in methanol to obtain HB-PAM-1. The atomic force microscopy (AFM) image of the chloroform dispersion of HB-PAM-1 dropcast onto a glass substrate revealed the formation of nanoparticles of diameter *ca.* 300 nm (Fig. 4a).

Since ACN is a bad solvent for the growth of higher dimensional conjugated polymers, we expected that well-defined HB-PAM nanoparticles can be obtained by increasing the percentage of ACN in the reaction mixture. Consequently, we systematically increased the percentage of ACN in the reaction mixture for generating HB-PAMs as shown in Table 3. After a two-hour reaction time, the resulting dispersions were dropcast onto a glass substrate and visualized using AFM. Contrary to our expectations, as the percentage of ACN increased, aggregates and thick films were observed under AFM. This indicates that using ACN as a co-solvent for HB-PAM synthesis is ineffective even though it was helpful in the case of the synthesis of linear polymers (*p*-PAM and *m*-PAM).

Lastly, the concentration of DADA was reduced to 2 mM and only CHCl<sub>3</sub> was used as the solvent (Table 4). The resultant particles after 90 minutes (HB-PAM-2) and 2 hours (HB-PAM-3) were analyzed using AFM. In both the cases, the resultant HB-PAM nanoparticles were dispersible in CHCl<sub>3</sub>. The AFM images of HB-PAM-2 and 3 are shown in Fig. 4b and c, respectively. HB-PAM-2 showed nanoparticles of diameter *ca.* 60 nm (Fig. 4b), whereas an increase in the polymer growth time resulted in particles (HB-PAM-3) of a relatively larger size but with irregular geometry, *~*90 nm (Fig. 4c).

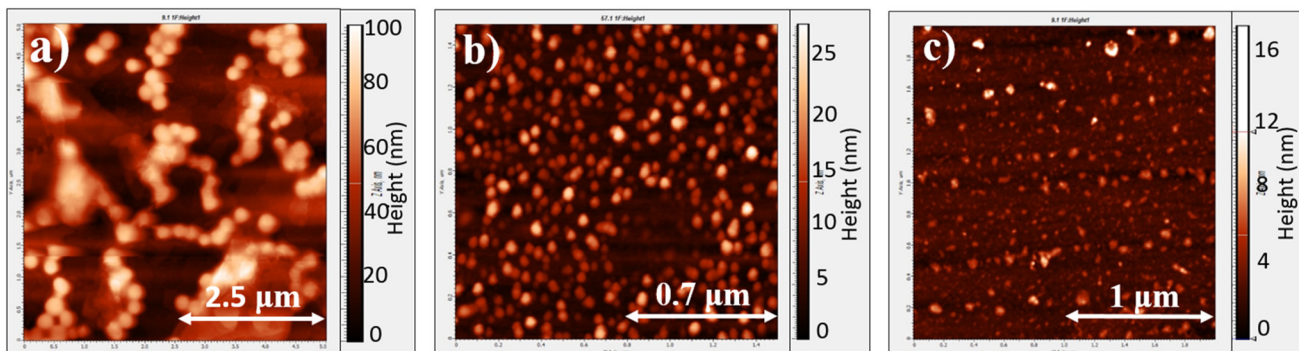


**Fig. 4** AFM images of (a) HB-PAM-1, (b) HB-PAM-2 and (c) HB-PAM-3.

**Table 3** Effect of ACN as a co-solvent with  $\text{CHCl}_3$  on the synthesis of HB-PAM

% of ACN	33%	50%	66%	100%
Observation	Dispersion	Dispersion	Dispersion	Dispersion
Monomer concentration: 4.2 mM; catalyst: $\text{CH}_3\text{COOH}$ ; time: 2 h.				

**Table 4** Effect of 2 mM monomer concentration in  $\text{CHCl}_3$  on the synthesis of HB-PAM

	Catalyst	Time	Observation
(i)	Acetic acid	90 m	Dispersion (HB-PAM-2)
(ii)	Acetic acid	2 h	Dispersion (HB-PAM-3)

Structural analysis of HB-PAM was done using ATR-IR and solution-state  $^1\text{H}$  NMR. Fig. 5a and S2 $\dagger$  show the ATR-IR spectra of HB-PAM-1. Similar to *m*-PAM, the appearance of a new peak at around  $1620\text{ cm}^{-1}$  is due to the  $\text{C}=\text{N}$  stretch in HB-PAM-1 and confirms the imine formation. The low-intensity aldehyde stretch at  $1690\text{ cm}^{-1}$ , similar to that observed in linear *m*-PAM, is attributed to the terminal aldehyde groups. The  $^1\text{H}$  NMR spectrum of the HB-PAM-1 dispersion is shown in Fig. 5b and S10. $\dagger$  As anticipated, the peaks in the NMR spectrum of HB-PAM-1 display broadening, indicating the formation of the polymer. The low intensity peak at  $10.35\text{ ppm}$  is attributed to the terminal aldehyde groups (Fig. S10 $\dagger$ ). The peak corresponding to the imine protons is observed at  $8.83\text{ ppm}$  for HB-PAM-1 (Fig. 5b). Notably, this peak exhibited two shoulders on either side, distinguishing it from the single peak observed in the  $^1\text{H}$  NMR spectra of the linear polyazomethines (*p*-PAM and *m*-PAM). Depending on the number of amines on the 1,3,5-benzenetriamine reacted, the HB-PAM will have dendritic (all three amines reacted), linear (two amines reacted), and terminal (one amine reacted) groups. To better understand the  $^1\text{H}$  NMR spectrum of HB-PAM-1, a model trimer was synthesized by reacting 1,3,5-benzenetriamine with compound 7 (see the ESI $\dagger$ ). In the model trimer, all amines on the 1,3,5-benzenetriamine are converted into imines and the imine proton is observed as a singlet at  $8.78\text{ ppm}$  (Fig. S12 $\dagger$ ). In the case of the *m*-PAM linear polymer, the two amines on the *m*-phenylenediamine are converted into imines and the imine proton chemical shifts are at  $8.9\text{ ppm}$  (Fig. S9 and S13 $\dagger$ ). Therefore, the chemical shift of the imine proton moves upfield as the greater number of amines in 1,3,5-benzenetriamine convert into imines.<sup>58,59</sup> Based on the chemical shifts of the model trimer and *m*-PAM, the peaks at  $8.93$ ,  $8.83$  and  $8.74\text{ ppm}$  are assigned to the terminal (T), linear (L), and dendritic (D) groups, respectively, as shown in Fig. 5b. The degree of branching (DB) for HB-PAM can be calculated from the percentage of each of these groups. The DB of HB-PAM-1 was calculated using the equation  $\text{DB} = (\text{T} + \text{D})/(\text{T} + \text{D} + \text{L})$ , developed by Frechet *et al.*<sup>60</sup>, and is found to be  $0.46$  for HB-PAM-1, which indicates a hyperbranched architecture. DB informs about the

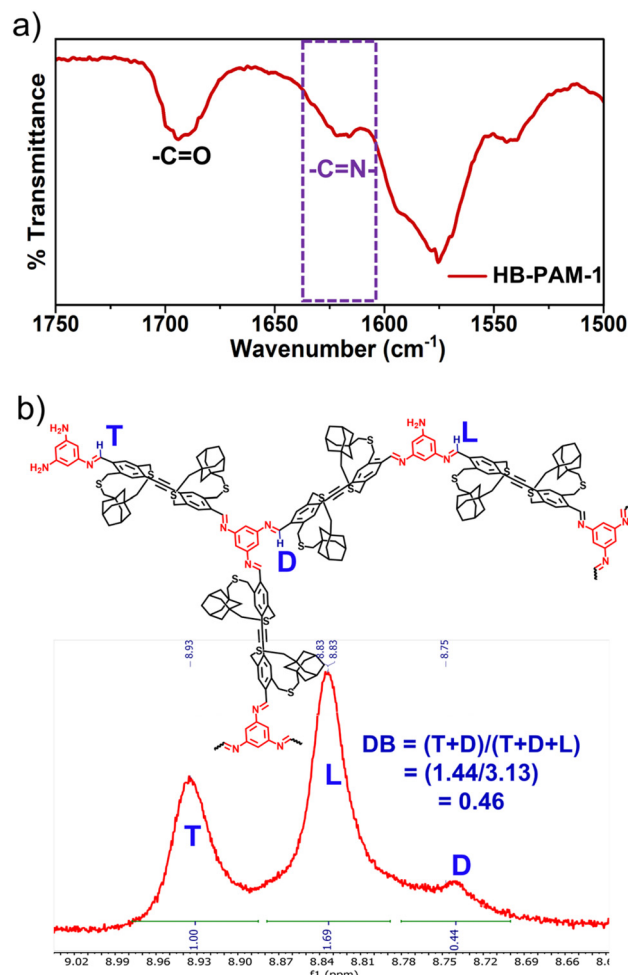


**Fig. 5** (a) ATR-IR spectra of HB-PAM-1 highlighting the imine bond formation; (b)  $^1\text{H}$  NMR spectrum of HB-PAM-1 in  $\text{CDCl}_3$  from  $8.5$  to  $9.0\text{ ppm}$  highlighting the imine formation and calculation of degree of branching from peak integrations.

topology and architecture of the polymer; typically polymers with the DB in the range between  $0.35$  and  $0.65$  are considered as hyperbranched polymers. A high DB suggests that the topological structure of the polymer is comparable to dendrimer analogues, whereas a low DB indicates that the structure is analogous to a linear polymer.<sup>61,62</sup>

The powder X-ray diffraction (PXRD) pattern of HB-PAM-1 (Fig. S3 $\dagger$ ) does not show any sharp peaks, indicating that the polymer is amorphous in nature. The two broad peaks centered around  $2\theta = 11.58$  and  $18.74$ , correspond to  $7.6\text{ \AA}$  and  $4.7\text{ \AA}$ , respectively. Based on the PXRD of our previously reported adamantanocyclophane Glaser-Hay 1D-homopolymer,  $7.6\text{ \AA}$  corresponds to the height of the adamantane straps and hence to the interlayer distance between the polymer chains.<sup>37</sup> Since the straps on the DADA building block mask the  $\pi$ -face of the monomer, they effectively hinder the  $\pi$ -stacking interactions between the oligomers, thereby obstructing the formation of ordered aggregates and hence the formation of crystalline covalent organic frameworks (COFs).

Instead, the oligomers assume a 3D architecture as they grow similar to dendrimers and result in the formation of a  $\pi$ -conjugated hyperbranched polymer. Solution processable hyperbranched conjugated polymers have been synthesized using repeat units that contain pendant solubilizing chains.<sup>21,24,27,28</sup> However, solution soluble hyperbranched polymers without the pendant solubilizing chains are not known to the best of our knowledge. The nearest systems to the hyperbranched conjugated polymers without pendant solubilizing chains are conjugated (porous) polymer networks. Conjugated polymer networks due to the absence of solubilizing pendant chains become insoluble aggregates as the degree of polymerization increases. This is attributed to the strong interchain interactions ( $\pi$ - $\pi$  and van der Waals interactions) within the network.<sup>15-18</sup> Cooper and other research groups generated soluble low molecular weight hyperbranched polyarylenes by taking advantage of the interarylene torsion angle and pendant solubilizing chains.<sup>19,29-31</sup> The interarylene torsion angle along with the pendant solubilizing chains reduces interchain interactions and results in low molecular weight, soluble, hyperbranched polymers. Typically, dispersible hyperbranched conjugated polymer particles are synthesized using the miniemulsion technique, wherein the surfactant acts as a stabilizer.<sup>19-25</sup> In this work, we observed that the straps generate hyperbranched polymers that are dispersible in chloroform without pendant solubilizing chains or surfactants. The straps prevent the extensive aggregation of polymer chains, leading to the formation of a dispersible hyperbranched polymer.

An interesting observation regarding the morphology of the nanoparticles is that they all exhibit pancake like morphology, *i.e.*, the diameter of the nanoparticles is higher than the height of the particles (Fig. 4). The diameter and height of HB-PAM-1-3 are  $300 \times 60$ ,  $60 \times 10$ , and  $90 \times 6$  nm, respectively. Thus, the diameter of the HB-PAM nanoparticles ranges from 60 to 300 nm, whereas the height of the nanoparticles ranges from 6 to 60 nm. The pancake morphology is observed here because the polymer architecture is unable to self-support its hyper-branched structure, leading to collapse onto itself. This pancake morphology has also been observed in dendrimers, which are considered as analogs of defect-free hyperbranched polymers in the  $A_2 + B_3$  system, as well as in hyperbranched polymers.<sup>63,64</sup> It is known that dendritic polymers with a low branching density adopt a disk-like morphology when drop-coated onto substrates. For example, arborescent graft polystyrene with a low branching density cannot self-sustain the structure and flattens due to adsorption forces with the substrate.<sup>65</sup> Similarly, dendrimers have exhibited a pancake-like morphology for analogous reasons, as shown by research conducted by the Zimmerman group and others.<sup>63,64</sup> This pancake morphology has also been observed in specific cases of conjugated hyperbranched polymers/conjugated porous polymers, where the width exceeded the height of particles by at least 3–5 times.<sup>1,66,67</sup> In contrast to low branching density non-conjugated HBPs and dendrimers, the relatively more rigid backbone of conjugated polymers aids in maintaining their structure in the solid state. This is evident through the

porosity measurements done on the conjugated porous networks, where high porosity is observed for highly crosslinked porous network structures.<sup>11</sup> However, as the network density (branching density) decreases, the intrachain interactions ( $\pi$ - $\pi$  and van der Waals interactions) dominate, which lead to the collapse of the network and low porosity.<sup>11</sup> Therefore, the disk-shaped morphology observed in the reported HBPs can be attributed to the significant interchain interactions in the solid state, combined with the relatively low branching density, drawing parallels to observations from the literature on non-conjugated dendrimers, HBPs and conjugated porous networks. The higher surface area to volume ratio of HB-PAMs resulting from the pancake morphology is advantageous for effective interaction with small molecule dopants for electronic and semiconducting applications.<sup>41,68,69</sup>

The UV-vis absorption and photoluminescence spectra of *p*-PAM, *m*-PAM and HB-PAM-1 in  $\text{CHCl}_3$  are shown in Fig. 6 and their optical properties are summarized in Table 5. The absorption maximum for *p*-PAM is at 423 nm, while the absorption maximum for *m*-PAM is at 387 nm. In *p*-PAM, the repeat units are connected by *p*-phenylenediamine, which extends the  $\pi$ -conjugation, hence showing a higher absorption maximum compared to *m*-PAM wherein the repeat units are connected by *m*-phenylenediamine. The absorption maximum of HB-PAM-1 is observed at 389 nm, which is similar to that of *m*-PAM, likely due to the limited electron delocalization in

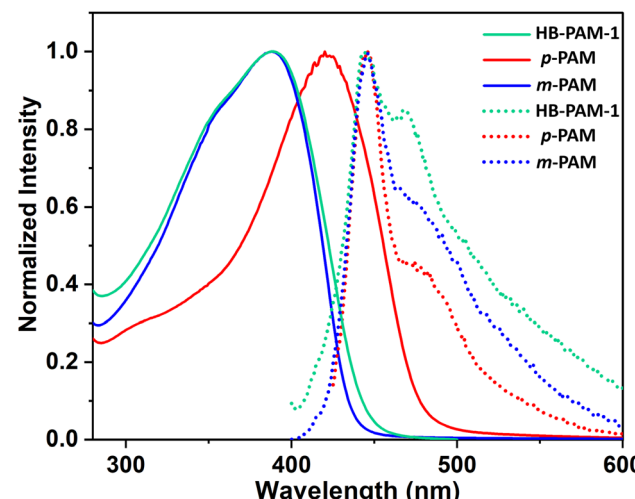


Fig. 6 Normalized UV-vis (solid lines) and photoluminescence (dotted lines) spectra of *p*-PAM, *m*-PAM and HB-PAM-1 in  $\text{CHCl}_3$ .

Table 5 Summary of optical properties of PAMs and HB-PAM-1

Polymer	Absorbance max (nm)	Emission max (nm)	Stokes shift (nm)	$I_{475}/I_{450}$
<i>p</i> -PAM	423	445	22	0.45
<i>m</i> -PAM	387	445	58	0.62
HB-PAM-1	389	443	54	0.85

both compounds due to the *meta*-connection between the repeat units.

In contrast to the trend observed in the absorption maxima, the photoluminescence spectra of *p*-PAM, *m*-PAM, and HB-PAM-1 are similar, with emission maxima at around 445 nm and a shoulder peak at around 475 nm. This peak feature is similar to that observed in previously reported adamantanocyclophane-based Glaser–Hay 1D-homopolymers.<sup>37</sup> The Stokes shift for *p*-PAM is 22 nm, while the Stokes shift for *m*-PAM and HB-PAM-1 is approximately 55 nm. A larger Stokes shift in the case of *m*-PAM and HB-PAM-1 suggests that the exciton delocalizes to a lower energy configuration upon excitation. All three polymers showed a difference in the ratio of the intensity of the emission peak at 475 with respect to 445 nm as shown in Fig. 6 and Table 5. The  $I_{475}/I_{450}$  value increases in the order *p*-PAM < *m*-PAM < HB-PAM-1 and can be correlated to the reduced conformational freedom along the polymer backbone.

## Conclusions

In summary, the efficacy of cycloalkyl straps in masking the  $\pi$ -face is demonstrated by the design and synthesis of  $\pi$ -face strapped building blocks that enabled the production of solution-dispersible and processable hyperbranched polyazomethines (HB-PAMs) without the necessity of incorporating pendant solubilizing chains or use of surfactants (Fig. 1). This work represents a significant advancement in hyperbranched polymer synthesis. The straps mask the  $\pi$ -face of the monomer effectively, hindering the  $\pi$ -stacking interactions between the oligomers and thereby obstructing the formation of ordered aggregates and formation of crystalline COFs. Instead, the oligomers assume a 3D architecture as they grow similar to dendrimers and result in the formation of a  $\pi$ -conjugated hyperbranched polymer. Since straps stabilize the chains against  $\pi$ – $\pi$  interactions at the molecular level, they will not only provide synthetic control over the architecture but also remove typical synthetic limitations associated with the miniemulsion technique including functional group intolerance and monomer miscibility. The generated hyperbranched polymer particles exhibit a distinctive pancake morphology, which offers a higher surface area to volume ratio. The extended  $\pi$ -conjugation beyond a 1D-chain along with the high surface area of a pancake morphology will facilitate efficient interactions between the hyperbranched polymer and small molecules (acceptors, analytes, and dopants). This will help to unlock the potential of hyperbranched polymers and lead to exciting advancements in fields such as electronics, sensors, and energy conversion.

## Author contributions

M. M. performed synthesis, structural and optical characterization studies and was involved in data analysis and draft writing. X. Z. helped with AFM imaging. N. G. conceived the

idea, guided the experimental work, was involved in data analysis, and prepared the manuscript.

## Conflicts of interest

There are no conflicts to declare.

## Acknowledgements

This work was supported by the National Science Foundation CAREER Grant (NSF-1944184) and Georgetown University. M. M. & N. G. thank Dr Jeffery A. Bertke for his help in crystal structure analysis of DADA. ChatGPT provided assistance in sentence editing.

## References

- 1 X. Liu, Y. Xu and D. Jiang, *J. Am. Chem. Soc.*, 2012, **134**, 8738–8741.
- 2 K. A. Mazzio and C. K. Luscombe, *Chem. Soc. Rev.*, 2015, **44**, 78–90.
- 3 D. T. McQuade, A. E. Pullen and T. M. Swager, *Chem. Rev.*, 2000, **100**, 2537–2574.
- 4 H. Zhou, L. Yang and W. You, *Macromolecules*, 2012, **45**, 607–632.
- 5 C. L. Anderson, H. Li, C. G. Jones, S. J. Teat, N. S. Settineri, E. A. Dailing, J. Liang, H. Mao, C. Yang, L. M. Klivansky, X. Li, J. A. Reimer, H. M. Nelson and Y. Liu, *Nat. Commun.*, 2021, **12**, 6818.
- 6 M. G. Mohamed, A. F. M. El-Mahdy, M. G. Kotp and S.-W. Kuo, *Mater. Adv.*, 2022, **3**, 707–733.
- 7 J. W. Colson and W. R. Dichtel, *Nat. Chem.*, 2013, **5**, 453–465.
- 8 J. Guo, Y. Xu, S. Jin, L. Chen, T. Kaji, Y. Honsho, M. A. Addicoat, J. Kim, A. Saeki, H. Ihee, S. Seki, S. Irle, M. Hiramoto, J. Gao and D. Jiang, *Nat. Commun.*, 2013, **4**, 1–8.
- 9 Y. Xu, S. Jin, H. Xu, A. Nagai and D. Jiang, *Chem. Soc. Rev.*, 2013, **42**, 8012.
- 10 Y. Byun and A. Coskun, *Chem. Mater.*, 2015, **27**, 2576–2583.
- 11 J.-S. M. Lee and A. I. Cooper, *Chem. Rev.*, 2020, **120**, 2171–2214.
- 12 Y. Tian and G. Zhu, *Chem. Rev.*, 2020, **120**, 8934–8986.
- 13 G. A. Leith, C. R. Martin, A. Mathur, P. Kittikhunnatham, K. C. Park and N. B. Shustova, *Adv. Energy Mater.*, 2021, **12**, 2100441.
- 14 S. Xu and Q. Zhang, *Mater. Today Energy*, 2021, **20**, 100635.
- 15 W. Wu, R. Tang, Q. Li and Z. Li, *Chem. Soc. Rev.*, 2015, **44**, 3997–4022.
- 16 D. Taylor, S. J. Dalgarno, Z. Xu and F. Vilela, *Chem. Soc. Rev.*, 2020, **49**, 3981–4042.
- 17 A. Laybourn, R. Dawson, R. Clowes, T. Hasell, A. I. Cooper, Y. Z. Khimyak and D. J. Adams, *Polym. Chem.*, 2014, **5**, 6325–6333.

18 G. Cheng, B. Bonillo, R. S. Sprick, D. J. Adams, T. Hasell and A. I. Cooper, *Adv. Funct. Mater.*, 2014, **24**, 5219–5224.

19 S. Bandyopadhyay, P. Pallavi, A. G. Anil and A. Patra, *Polym. Chem.*, 2015, **6**, 3775–3780.

20 A. J. Kalin, S. Che, C. Wang, A. U. Mu, E. M. Duka and L. Fang, *Macromolecules*, 2020, **53**, 922–928.

21 H. Li, X. Wu, B. Xu, H. Tong and L. Wang, *RSC Adv.*, 2013, **3**, 8645.

22 B. C. Ma, S. Ghasimi, K. Landfester, F. Vilela and K. A. I. Zhang, *J. Mater. Chem. A*, 2015, **3**, 16064–16071.

23 P. Zhang, K. Wu, J. Guo and C. Wang, *ACS Macro Lett.*, 2014, **3**, 1139–1144.

24 X. Wu, Z. Zhang, H. Hang, Y. Chen, Y. Xu, H. Tong and L. Wang, *Macromol. Rapid Commun.*, 2017, **38**, 1700001.

25 P. Zhang, K. Wu, J. Guo and C. Wang, *ACS Macro Lett.*, 2014, **3**, 1139–1144.

26 C. P. Sen, V. D. Goud, R. G. Shrestha, L. K. Shrestha, K. Ariga and S. Valiyaveettil, *Polym. Chem.*, 2016, **7**, 4213–4225.

27 B. Wang, Q. Tan, J. Lu and H. Liang, *J. Polym. Sci., Part A: Polym. Chem.*, 2018, **56**, 96–104.

28 P. Zhou, C. Zhong, X. Chen, J. Qin, I. Mariz and E. Maçôas, *Macromolecules*, 2014, **47**, 6679–6686.

29 G. Cheng, T. Hasell, A. Trewin, D. J. Adams and A. I. Cooper, *Angew. Chem., Int. Ed.*, 2012, **51**, 12727–12731.

30 P. Pallavi, S. Bandyopadhyay, J. Louis, A. Deshmukh and A. Patra, *Chem. Commun.*, 2017, **53**, 1257–1260.

31 A. Deshmukh, S. Bandyopadhyay, A. James and A. Patra, *J. Mater. Chem. C*, 2016, **4**, 4427–4433.

32 J. Royakkers and H. Bronstein, *Macromolecules*, 2021, **54**, 1083–1094.

33 F. Cacialli, J. S. Wilson, J. J. Michels, C. Daniel, C. Silva, R. H. Friend, N. Severin, P. Samori, J. P. Rabe, M. J. O'Connell, P. N. Taylor and H. L. Anderson, *Nat. Mater.*, 2002, **1**, 160–164.

34 M. J. Frampton and H. L. Anderson, *Angew. Chem., Int. Ed.*, 2007, **46**, 1028–1064.

35 S. Pecorario, J. Royakkers, A. D. Scaccabarozzi, F. Pallini, L. Beverina, H. Bronstein and M. Caironi, *Chem. Mater.*, 2022, **34**, 8324–8335.

36 J. Royakkers, A. Minotto, D. G. Congrave, W. Zeng, A. Hassan, A. Leventis, F. Cacialli and H. Bronstein, *Chem. Mater.*, 2020, **32**, 10140–10145.

37 S. Chaudhuri, M. Mohanan, A. V. Willem, J. A. Bertke and N. Gavvalapalli, *Chem. Sci.*, 2019, **10**, 5976–5982.

38 R. Lillis, M. R. Thomas, M. Mohanan and N. Gavvalapalli, *Macromolecules*, 2021, **54**, 3112–3119.

39 F. Hameed, M. Mohanan, N. Ibrahim, C. Ochonma, J. Rodríguez-López and N. Gavvalapalli, *Macromolecules*, 2023, **56**, 3421–3429.

40 M. K. Das, F. Hameed, R. Lillis and N. Gavvalapalli, *Mater. Adv.*, 2020, **1**, 2917–2925.

41 M. Mohanan, H. Ahmad, P. Ajayan, P. K. Pandey, B. M. Calvert, X. Zhang, F. Chen, S. J. Kim, S. Kundu and N. Gavvalapalli, *Chem. Sci.*, 2023, **14**, 5510–5518.

42 J. F. S. Matthew and E. Belowich, *Chem. Soc. Rev.*, 2012, **41**, 2003–2024.

43 T. Ide, D. Takeuchi and K. Osakada, *Chem. Commun.*, 2012, **48**, 278–280.

44 Y. Jin, Q. Wang, P. Taynton and W. Zhang, *Acc. Chem. Res.*, 2014, **47**, 1575–1586.

45 X. Li, C. Zhang, S. Cai, X. Lei, V. Alton, F. Hong, J. J. Urban, J. Ciston, E. M. Chan and Y. Liu, *Nat. Commun.*, 2018, **9**, 2998.

46 K. D. Okochi, Y. Jin and W. Zhang, *Chem. Commun.*, 2013, **49**, 4418–4420.

47 P. She, Y. Qin, X. Wang and Q. Zhang, *Adv. Mater.*, 2022, **34**, 2101175.

48 J. M. Rotter, R. Guntermann, M. Auth, A. Mahringer, A. Sperlich, V. Dyakonov, D. D. Medina and T. Bein, *Chem. Sci.*, 2020, **11**, 12843–12853.

49 Y. Jin, C. Yu, R. J. Denman and W. Zhang, *Chem. Soc. Rev.*, 2013, **42**, 6634–6654.

50 H. Xu, J. Gao and D. Jiang, *Nat. Chem.*, 2015, **7**, 905–912.

51 A. Bolduc, A. Al Ouahabi, C. Mallet and W. G. Skene, *J. Org. Chem.*, 2013, **78**, 9258–9269.

52 A. Bolduc, S. Dufresne and W. G. Skene, *J. Mater. Chem.*, 2012, **22**, 5053.

53 S. Barik, T. Bletzacker and W. G. Skene, *Macromolecules*, 2012, **45**, 1165–1173.

54 S. Barik, D. Navarathne, M. LeBorgne and W. G. Skene, *J. Mater. Chem. C*, 2013, **1**, 5508.

55 M. Faheem, S. Aziz, X. Jing, T. Ma, J. Du, F. Sun, Y. Tian and G. Zhu, *J. Mater. Chem. A*, 2019, **7**, 27148–27155.

56 F. Qureshi, S. Q. Memon, M. Y. Khuhawar, T. M. Jahangir and A. H. Channar, *J. Polym. Res.*, 2021, **28**, 259.

57 P. H. Salunkhe, Y. S. Patil, V. B. Patil, Y. H. Navale, I. A. Dhole, V. P. Ubale, N. N. Maldar and A. A. Ghanwat, *J. Polym. Res.*, 2018, **25**, 147.

58 S. A. P. Guarin and W. G. Skene, *Mater. Lett.*, 2007, **61**, 5102–5106.

59 P. Nitschke, B. Jarząbek, A. Wanic, M. Domański, B. Hajduk, H. Janeczek, B. Kaczmarczyk, M. Musioł and M. Kawalec, *Synth. Met.*, 2017, **232**, 171–180.

60 C. J. Hawker, R. Lee and J. M. J. Fréchet, *J. Am. Chem. Soc.*, 1991, **113**, 4583–4588.

61 H. Chen and J. Kong, *Polym. Chem.*, 2016, **7**, 3643–3663.

62 A. L. Brigitte and I. Voit, *Chem. Rev.*, 2009, **109**, 5924–5973.

63 N. G. Lemcoff, T. A. Spurlin, A. A. Gewirth, S. C. Zimmerman, J. B. Beil, S. L. Elmer and H. G. Vandeveer, *J. Am. Chem. Soc.*, 2004, **126**, 11420–11421.

64 P. Taranekar, J. Y. Park, D. Patton, T. Fulghum, G. J. Ramon and R. Advincula, *Adv. Mater.*, 2006, **18**, 2461–2465.

65 S. S. Sheiko, M. Gauthier and M. Möller, *Macromolecules*, 1997, **30**, 2343–2349.

66 C. Gu, N. Huang, Y. Chen, L. Qin, H. Xu, S. Zhang, F. Li, Y. Ma and D. Jiang, *Angew. Chem.*, 2015, **127**, 13798–13802.

67 M. Xu, X. Han, T. Wang, S. Li and D. Hua, *J. Mater. Chem. A*, 2018, **6**, 13894–13900.

68 H. Veldhuijen, L. Elzen, T. Mahon, R. Abellon and A. Nagai, *Macromol. Chem. Phys.*, 2020, **221**, 1900415.

69 K. V. Rao, S. Mohapatra, T. K. Maji and S. J. George, *Chemistry*, 2012, **18**, 4505–4509.